CONTINUUM EXCITATIONS IN ^{6}He

T. Aumann, D. Aleksandrov, L. Axelsson, T. Baumann, M.J.G. Borge, L.V. Chulkov,
J. Cub, W. Dostal, B. Eberlein, Th.W. Elze, H. Emling, H. Geissel, V.Z. Goldberg,
M. Golovkov, A. Grünschloß, M. Hellström, K. Hencken, J. Holeczek, R. Holzmann,
B. Jonson, A.A. Korshenninikov, J.V. Kratz, G. Kraus, R. Kulessa, Y. Leifels,
A.Leistenschneider, T. Leth, I. Mukha, G. Münzenberg, F. Nickel, T. Nilsson,
G. Nyman, B. Petersen, M. Pfützner, A. Richter, K. Riisager, C. Scheidenberger,
G. Schrieder, W. Schwab, H. Simon, M.H. Smedberg, M. Steiner, J. Stroth,
A. Surowiec, T. Suzuki, O. Tengblad, M.V. Zhukov

Continuum Excitations in ^{6}He

T. Aumann[1,2,3], D. Aleksandrov[4], L. Axelsson[5], T. Baumann[2], M.J.G. Borge[6], L.V. Chulkov[4], J. Cub[2,7],
W. Dostal[1], B. Eberlein[1], Th. W. Elze[8], H. Emling[2], H. Geissel[2], V. Z. Goldberg[4], M. Golovkov[4], A. Grünschloß[8],
M Hellström[2], K. Hencken[9], J. Holeczek[2,10], R. Holzmann[2], B. Jonson[5], A. A. Korshenninikov[11], J. V. Kratz[1],
G. Kraus[2], R. Kulessa[12], Y. Leifels[2], A. Leistenschneider[8], T. Leth[13], I. Mukha[4,13], G. Münzenberg[2], F. Nickel[2],
T. Nilsson[5], G. Nyman[5], B. Petersen[13], M. Pfützner[2], A. Richter[7], K. Riisager[13], C. Scheidenberger[2], G. Schrieder[7],
W. Schwab[2], H. Simon[7], M. H. Smedberg[5], M. Steiner[3], J. Stroth[8], A. Surowiec[2,10], T. Suzuki[11], O. Tengblad[6] and
M. V. Zhukov[5]

[1] Institut für Kernchemie, Johannes Gutenberg-Universität, D–55099 Mainz, Germany
[2] Gesellschaft für Schwerionenforschung (GSI), Planckstr. 1, D–64291 Darmstadt, Germany
[3] Michigan State University, East Lansing, MI 48824-1321, USA
[4] Kurchatov Institute, RU–123182 Moscow, Russia
[5] Fysiska Institutionen, Chalmers Tekniska Högskola and Göteborgs Universitet, S–412 96 Göteborg, Sweden
[6] Instituto Estructura de la Materia, CSIC, E–28006 Madrid, Spain
[7] Institut für Kernphysik, Technische Universität, D–64289 Darmstadt, Germany
[8] Institut für Kernphysik, Johann-Wolfgang-Goethe-Universität, D–60486 Frankfurt, Germany
[9] Department für Physik und Astronomie, Universität Basel, CH–4056 Basel, Switzerland
[10] Instytut Fizyki, Uniwersytet Śląski, PL-40-007 Katowice, Poland
[11] RIKEN, 2-1 Hirosawa, Wako, Saitama 351-01, Japan
[12] Instytut Fizyki, Uniwersytet Jagielloński, PL-30-059 Kraków, Poland
[13] Institut for Fysik og Astronomi, Aarhus Universitet, DK–8000 Aarhus C, Denmark

The three-body break-up ^{6}He $\rightarrow$ ^{4}He $+ n + n$ is studied experimentally, using a secondary ^{6}He ion beam of 240 MeV/u incident on carbon and lead targets. Integrated cross sections for one- and two-neutron knock-out and differential cross sections $d\sigma/dE^*$ and $d\sigma/d\vartheta$ for inelastic nuclear or electromagnetic excitations into the ^{6}He continuum are presented. The E1-strength distribution is deduced from electromagnetic cross sections and is found to exhaust $(10 \pm 2)\%$ of the energy-weighted TRK sum rule or $(40 \pm 8)\%$ of the cluster sum rule for excitation energies below 5 MeV. Both the energy-weighted and non-energy-weighted dipole cluster sum rules are almost exhausted integrating the strength up to 10 MeV, a fact, from which a root-mean-square distance between the α core and the two valence neutrons of $r_{\alpha-2n} = (3.36 \pm 0.29)$ fm is derived. The known $I^\pi = 2^+$ (1.80 MeV) resonance in ^{6}He is observed in nuclear inelastic scattering; model dependent values of the quadrupole deformation parameter $\delta_2 = (1.7 \pm 0.3)$ fm or $B(E2, 0^+ \rightarrow 2^+) = (3.2 \pm 0.6)$ e^2fm^4 are derived. No clear signature could be obtained for predicted higher-lying 2^+ resonances, but low-lying continuum strength of multipolarity other than dipole, likely of monopole and quadrupole multipolarity, is indicated by the data. Two–body correlations in the decaying ^{4}He $+ n + n$ system are investigated. The astrophysical relevance of the data with regard to the two-neutron capture process ^{4}He$(2n,\gamma)^6$He is briefly discussed.

PACS number(s): 27.20.+n, 25.60.+v, 25.70.De, 29.30.hs

I. INTRODUCTION

Continuum excitations play a key role in exploring the single-particle and collective structure of weakly bound nuclei located near the driplines. Such nuclei have very few or no bound excited states, and thus, a study of transitions to resonances embedded into the continuum replaces, in some sense, the discrete level spectroscopy applicable in strongly bound nuclei. Furthermore, quite in contrast to properties known for stable nuclei, a considerable low-lying multipole strength has been predicted [1-7]. Low-lying dipole components, in fact, were observed experimentally in the neutron-halo nuclei ^{11}Li [8-10] and ^{11}Be [11]. The origin of multipole strength close to the break-up threshold is found, in a single-particle approach, in the optimal matching of the wavelength of the continuum scattering state with the valence nucleon wave function, penetrating far into classically forbidden regions. Although of non-resonant character, the associated strength distribution may still be characteristic of the specific ground state single-particle structure [12]. The role of coherent excitations, i.e. low-frequency oscillations of halo nucleons against the residual core in their weak mutual field, were alternatively discussed in Refs. [13-15].

It was suggested, moreover, that break-up reactions may give access to study correlations among loosely bound valence (halo) nucleons, arising from residual interactions [16]. Borromean-type nuclei such as ^{6}He, where each of the two-body subsystems is unstable, are evidently only stabilized by such forces. In high-energy break-up reactions, under circumstances allowing for a description of the reaction dynamics in the sudden approximation, initial-state two- or three-body correlations

were expected to be reflected in momentum correlations between the break-up residues.

A study of the ^{6}He break-up may also deliver data which are of astrophysical relevance with regard to the stellar nucleosynthesis. The two-neutron capture ^{4}He$(2n,\gamma)^6$He was discussed in the literature as a possible route bridging the instability gap at mass A= 5 [17,18]. We shall show that the inverse break-up reaction provides information relevant for calculating neutron-capture rates.

The present experimental study is devoted to ^{6}He, which is known to exhibit a neutron halo formed mainly by two $p_{3/2}$ neutrons outside the α core. The difference in proton and neutron rms radii was estimated to (0.61 ± 0.21) fm in Ref. [19] and to (0.93 ± 0.06) fm in Ref. [20]. The threshold for ^{6}He break-up into $\alpha + n + n$ is found at 975 keV, while ^{5}He is unbound [21]. Thus, ^{6}He appears to be an ideal study case in exploring the effects discussed above, having in mind as well that ^{6}He has been subject to numerous theoretical studies comprising the shell model approach, cluster models, and 'ab-initio' many-body calculations based on nucleon-nucleon scattering data and including three-body forces (see Refs. [22–25] and references therein). The experiment, in a first place, is aiming at identifying low-lying multipole strength, and sets out to investigate correlations between the decay residues in a measurement which is kinematically complete in the three-body channel $\alpha + n + n$.

II. EXPERIMENTAL METHOD AND DATA ANALYSIS

The secondary ^{6}He ion beam (240 MeV/u) was produced in a fragmentation reaction utilizing a primary ^{18}O beam (340 MeV/u) delivered by the synchrotron SIS at GSI, Darmstadt, and a beryllium target of 8 g/cm^2 thickness. The ^{6}He fragments were separated in the fragment separator FRS [26] and then transported to the experimental area. For isotope separation a degrader acting as a dispersive element was inserted in the midplane of the FRS. Contaminants in the secondary beam were observed on a few percent level only. Beam-ions incident on the secondary target (1.87 g/cm^2 C or 0.87 g/cm^2 Pb) were uniquely identified by means of an energy-loss measurement in a Si pin-diode and a time-of-flight measurement using thin organic scintillators. The trajectory of the secondary beam was determined by two multi-wire proportional counters (MWPC). Typically, a beam intensity of 10^3 ions/s was obtained. Behind the secondary target, the ^{4}He fragments were deflected by a large-gap dipole magnet. The nuclear charge of the fragments was obtained by a second Si pin-diode detector placed downstream close to the target. A third MWPC located between target and magnet served to determine the scattering angle ϑ of the fragments (resolution σ_ϑ=3.2 mrad).

Their time of flight (ToF) was measured in an array of 20 organic scintillators with an active area of 2 x 2 m^2 placed about 12.5 m downstream from the target (resolution $\sigma_{ToF} = 300$ ps including the velocity spread of the beam). The acceptance in transverse momentum for the α particles was limited to about -200 MeV/c $\leq p_x \leq 180$ MeV/c and -100 MeV/c $\leq p_y \leq 140$ MeV/c. Neutrons were detected in the large-area neutron detector LAND [27] with an efficiency of (82 ± 7)% in case of a single neutron hit, an angular resolution of $\sigma_\vartheta \approx 3$ mrad, and a time-of-flight resolution of $\sigma_{ToF} = 250$ ps. LAND consists of two hundred separate detector elements, allowing for multiple-hit recognition. The acceptance in transverse neutron momentum was limited to about -50 MeV/c $\leq p_{x,y} \leq 50$ MeV/c. Coincidences between a charged fragment and at least one neutron were selected by a fast trigger decision and were registered. Events triggered by any incident beam ion were registered in a down-scaled mode. This event class served for normalization to beam intensity, but was also used to measure reactions in the target without a coincident neutron. Results from this experiment concerning other physical aspects than considered here were published in Refs. [28,29].

As a first step during the data analysis, the α particle was identified and the 4−momentum components of the α particle and the coincident neutrons were determined (examples of α- or neutron-momentum distributions are found in Ref. [29]). The events were then discriminated according to the apparent neutron multiplicity $m_n = 0,1,2$ registered in LAND. As shall be outlined below, the apparent neutron multiplicity characterizes the reaction mechanism. For each neutron multiplicity, integrated cross sections were determined, taking into account corrections for the detection efficiency and limited acceptance (see above). For the acceptance correction the momentum distributions of the α particles and neutrons measured within the acceptance were parameterized appropriately and extrapolated. Acceptance corrections for the α particles amounted to typically 20% for both targets and all neutron multiplicities except for neutron multiplicity m_n=2 with the Pb target where the correction was found to be 2.5% only. A specific problem is related to the neutron detection: Neutrons impinging onto LAND fire a number of its sub-modules and a pattern recognition algorithm has to be employed in order to disentangle multiple neutron hits. The algorithm and its performance, under the circumstances of an experiment very similar to the present one, is described in Ref. [10]. The main effect appears in a reduced double-hit recognition capability in the case where two neutrons interact in close vicinity to each other in LAND. Such detection deficiencies were corrected for on the basis of realistic event simulations, adjusted to the present experiment, and utilizing the LAND response from calibration measurements with tagged neutrons. A correction for reactions taking place outside the target, e.g. in the detector material, was

accomplished by means of a measurement without target. Data from this measurement were analyzed in the same manner as those obtained with target and were subtracted after proper normalization from all spectra. In a final step, correlations between the 4-momenta in the 3-body $\alpha + n + n$ system or in its two-body subsystems were analyzed. To a large extent, we rely on the Lorentz invariant quantity $\sqrt{s} = \sqrt{(\sum_i p_i)^2}$, where p_i denotes the 4-momentum of particle i. The quantity $\sqrt{s} - \sum_i m_i^o$, where m_i^o is the rest mass, provides the total kinetic energy in the center-of-mass frame of the particles involved. In case of the decay of an excited nucleus, here ^{6}He with the ground state mass m_o, its excitation energy E^* is obtained simply as $E^* = \sqrt{s} - m_o$.

As we rely heavily on such excitation energy distributions for ^{6}He in Section IV, we present in Figure 1 the instrumental response of our detection system with regard to this quantity.

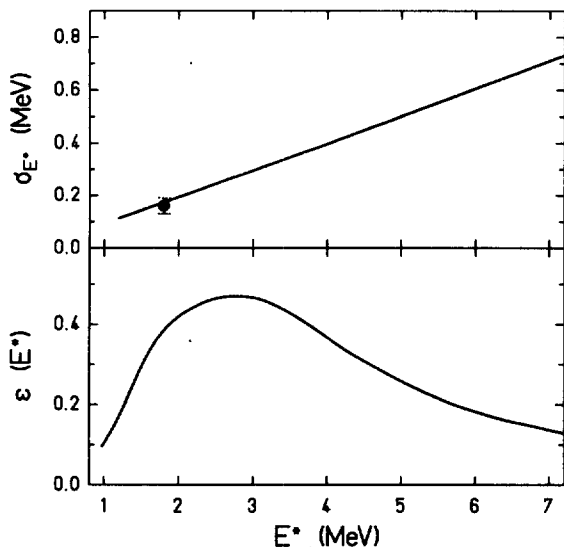FIG. 1. Overall resolution σ_{E^*} (top panel) and efficiency $\epsilon(E^*)$ (bottom panel) with regard to the excitation energy E^* of ^{6}He, obtained from event simulations (see text). The experimental value of the resolution at $E^* = 1.80$ MeV, shown in the top panel, was derived from the $I^\pi = 2^+$ resonance in ^{6}He observed with the C target.

to this quantity. The response for a given excitation energy of ^{6}He and subsequent decay into $\alpha + n + n$ is derived by the event simulation described above, taking into account intrinsic detection efficiencies, position resolutions, the time-of-flight resolution and finite acceptances for the α particle and the neutrons. The algorithm to disentangle the two neutrons impinging onto LAND is identical for the analysis of simulated and real events. For the event simulation, we assume zero momentum transfer to the excited ^{6}He and that the available kinetic energy is distributed among the α particle and the two neutrons according to standard phase space distributions. We have estimated that these simplifications give an uncertainty

of about 20 %. As shall be shown later, only small deviations from phase space distributions were observed in the experimental data. With this procedure, we obtain response functions which can be well described by Gaussian distributions. Small non-Gaussian wings are present on a few percent level which can be neglected under most circumstances. Experimentally, we were able to check the derived resolution from the $I^\pi = 2^+$ resonance at $E^* = 1.80$ MeV measured with the C target (see Section IV). The value of $\sigma_{E^*} = 0.16$ MeV is consistent with the value obtained in the event simulation, see Figure 1. The same procedure also delivers the detection efficiencies shown in Figure 1. The apparent decrease in efficiency, at low E^*, is due to the limited capability to resolve two neutrons with a small relative distance in LAND. The decrease at higher excitation energies is due to the finite solid angle acceptance.

III. REACTION MECHANISMS AND CROSS SECTIONS

Apart from excitations due to the nuclear or electromagnetic fields in distant collisions, nucleon knock-out processes occurring at close impact contribute substantially to the total break-up cross sections obtained at high bombarding energies. Inelastic excitations and knock-out reactions* can be distinguished in our experiment on the basis of the observed neutron multiplicity. For a detailed discussion in a related context, we refer to Ref. [10]. The main argument is that knock-out neutrons are scattered to large angles, thus escaping from detection in the limited forward angle cone covered by the neutron detector. In the present case of ^{6}He, a simultaneous knock-out of the two valence neutrons yields an apparent neutron multiplicity $m_n = 0$ and the knock-out of a single neutron yields $m_n = 1$. In the latter case, as shown in Ref. [29], the remaining $\alpha + n$ system forms the ^{5}He ground state resonance to a large extent. Due to the Lorentz boost, the decay neutron from this resonance falls within the acceptance of the neutron detector. In case of inelastic excitation into the continuum of ^{6}He, both decaying neutrons fall within the acceptance of LAND for excitation energies below about 4 MeV while the acceptance gradually decreases towards higher excitation energies, see Figure 1. Consequently, we may associate neutron multiplicites $m_n = 0, 1, 2$ to double knock-out and single knock-out, and inelastic excitations, respectively.

For these different reactions, integrated cross sections were extracted, applying corrections discussed in Sec-

_____

*We note that in the literature knock-out reactions and inelastic excitations are frequently referred to as stripping reactions and diffractive scattering, respectively.

3

tion II. The results are given in Table I for the C and

TABLE I. Measured integrated cross sections for inelastic excitation ($\sigma_{inel.}$), single- (σ_{-1n}), and two-neutron (σ_{-2n}) knock-out in ^{6}He (240 MeV/u) on C and Pb targets, leading to break-up into α and neutrons. The sum of all three cross sections (σ_{sum}) and the cross section for the $I^\pi = 2^+$ resonance at 1.80 MeV in ^{6}He are given as well. Errors include systematic and statistical ones. In case of the Pb target, the electromagnetic cross section ($\sigma_{e.m.}$) was estimated as discussed in the text.

σ (mb)	C target	Pb target
$\sigma_{inel.}$	30 ± 5	650 ± 110
σ_{-1n}	127 ± 14	320 ± 90
σ_{-2n}	33 ± 23	180 ± 100
$\sigma(2^+)$	4.0 ± 0.8	14 ± 4
σ_{sum}	190 ± 18	1150 ± 90
$\sigma_{e.m.}$		(520 ± 110)

Pb targets. In Figure 2, we compare these cross sections with the theoretical predictions of Ref. [30]. This calculation is based on the eikonal approximation which is appropriate at high energies. The cross sections were calculated for one- and two-neutron knock-out (in Ref. [30] referred to as "stripping") and for inelastic excitation (in Ref. [30] referred to as "diffractive" scattering) for ^{6}He (240 MeV/u) on a C target. The calculation takes into account recoil and core shadowing effects. The comparison of calculated and measured cross sections, displayed in Figure 2, shows perfect agreement. By applying the same theoretical method, we performed calculations for the Pb target as well, and the results are also shown in Figure 2. While the one- and two-neutron knock-out cross sections are reproduced within the experimental errors, we find a considerable excess for the experimental inelastic cross section. We attribute this excess in cross section to excitations in the strong electromagnetic field of the Pb target since electromagnetic processes are not considered in the model calculation. By comparing the measured and calculated cross sections, we derive a total electromagnetic cross section for ^{6}He with the Pb target of (520 ± 110) mb. We note that the nuclear inelastic cross sections obtained in eikonal approximation increase by a factor of 4, comparing that of the C target with the one of the Pb target, somewhat in excess of what would be obtained from a simple scaling with the nuclear radii. In turn, if we scale the electromagnetic cross section of the Pb target to that of the C target, adopting a Z_{target}^2 dependence, we derive the value 3 mb, being small in comparison to the measured inelastic cross section of (30 ± 5) mb.

Results from the knock-out reactions and their physics implications have already been presented in earlier publications [28,29]. The following section focuses on a discussion of the inelastic excitations.
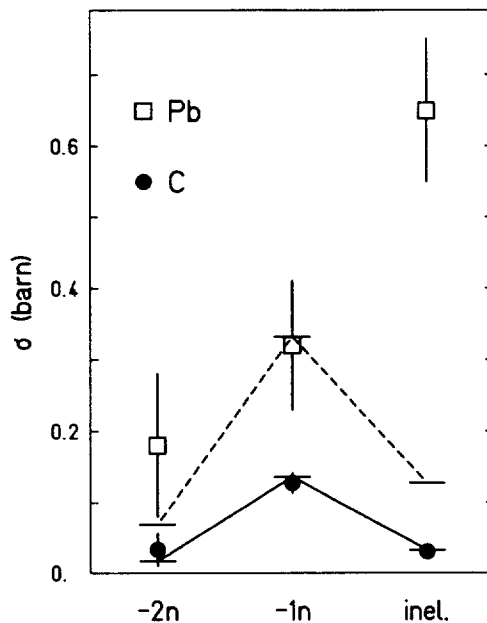

FIG. 2. Measured integrated cross sections for single- ($-1n$) and two-neutron ($-2n$) knock-out, and for inelastic excitation (inel.) in ^{6}He (240 MeV/u) on a C target (solid symbols) and a Pb target (open symbols), leading to break-up into α and neutrons. The solid and dashed lines connect the values from calculations in an eikonal model for the C target [30] and for the Pb target (see text), respectively. Electromagnetic excitations are not included in the model calculation.

IV. INELASTIC EXCITATIONS

As described in Section II, the excitation energy of ^{6}He can be derived from the invariant mass of the $\alpha + n + n$ system. The spectra are shown for the C and Pb targets in Figure 3. They are corrected for efficiency and solid angle acceptance, however, no attempt was made to fold out the energy resolution (see Section II). Since any deconvolution procedure enlarges statistical errors tremendously, we prefer to fold the response into calculated spectra if these are to be compared with the experimental data. For further theoretical comparisons, the experimental spectra and the detector response matrices which should be used to convolute calculated cross sections are provided upon request.

We point out that decay of ^{6}He into other channels than $\alpha + n + n$ can occur only at excitation energies above 12.3 MeV, which represents the threshold for decay into two tritons. The excitation energy spectra thus comprise the full strength for $E^* \leq 12.3$ MeV. As discussed in an earlier publication [29], the appearance of resonant structures may become enhanced in an appropriate correlation function, which eliminates residual effects due to detector response or finite solid angle acceptances. We follow the procedure outlined in [29] and refer to it for
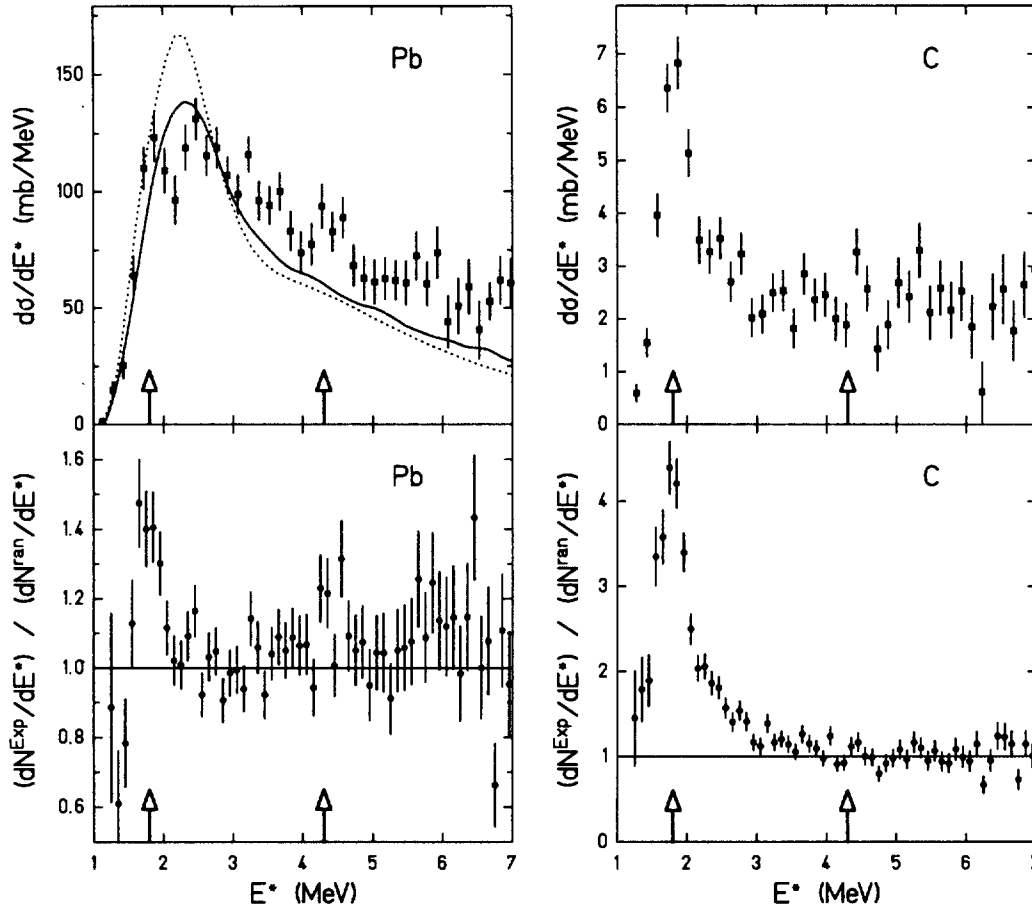
FIG. 3. Top: Excitation energy (E^*) spectra of ^{6}He deduced from the invariant mass of the $\alpha+n+n$ decay channel, obtained with the Pb target (left) and the C target (right) at 240 MeV/u bombarding energy. Differential cross sections $d\sigma/dE^*$ are given. The spectra are corrected for detection efficiency and solid angle acceptance, but they are not deconvoluted with respect to the resolution in E^* (see text). In case of the Pb target, the dotted curve represents the calculated electromagnetic cross section using the $dB(E1)/dE^*$ distribution from the three-body model of Ref.[7] and a semi-classical perturbative calculation. The solid curve is obtained by convoluting the dotted curve with the instrumental response. The excitation energies of a known ($E^* = 1.80$ MeV) and a predicted ($E^* = 4.3$ MeV [6] $I^\pi = 2^+$ resonance are indicated by arrows. Bottom: Corresponding correlation functions obtained as explained in the text.

details. The correlation function $R(E^*) = \frac{d\sigma/dE^*}{d\sigma^{ran}/dE^*}$, where $d\sigma^{ran}/dE^*$ denotes the excitation energy spectrum obtained from the invariant mass, was constructed by random combinations of α particles and neutrons from different events.

A. Electromagnetic scattering

We first concentrate on a discussion of the excitation energy spectrum and the respective correlation functions obtained with the Pb target. As was outlined in Section III, the major part of the cross section $\sigma_{inel.} = (650 \pm 110)$ mb obtained for the inelastic scattering on the Pb target can be assigned to electromagnetic excitation. The calculation of the nuclear contribution in the

eikonal approximation (see Section III), delivers 127 mb, i.e. a contribution of only 20 %.

In principle, the electromagnetic cross section may be composed of various multipolarities. Explicit multipole strength distributions for ^{6}He have been presented in Refs. [3,7,31] (see references therein) by deriving continuum state solutions of the three-body equations for the α core and two neutrons. The dipole ($I^\pi = 1^-$) strength distributions of Refs. [31] and [7] are shown in Figure 4. In a first step of the analysis, we used such theoretical strength distributions as input into a calculation of the electromagnetic cross section of the system under investigation applying the semi-classical method in the per-
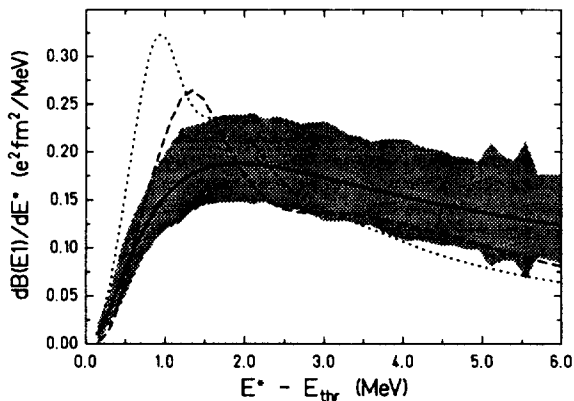
5

FIG. 4. Top: Dipole strength distributions adapted from Ref. [31] (dotted curve) and from Ref. [7] (dashed curve). The experimentally derived E1 strength distribution and the errors are given by the full drawn line and the broad band, respectively. The abscissa is the excitation energy E^* minus the two-neutron separation energy E_{thr}, the experimental value of which amounts to 0.975 MeV .

turbative approach as formulated in Ref. [32] [†]. The resulting cross sections for dipole excitation are compared with the measured data on an absolute scale in Figure 3. The magnitude of the measured cross section seems to be fairly well reproduced, keeping in mind that nuclear excitation processes are not taken into account. The cross section for the continuum electromagnetic quadrupole excitation, using the E2 strength distribution of Ref. [31], is found to contribute about 17 mb in total, thus being negligible. We expect that contributions from higher multipolarities are negligible as well.

In a second step of the analysis, we attempted to extract the dipole strength distribution directly from the data. For that purpose, we first corrected the experimental spectrum for contributions from nuclear excitations: The excitation energy spectrum obtained with the C target was multiplied with 4 and subtracted from that obtained with the Pb target. The scaling factor of 4 was deduced from the calculations in eikonal approximation as discussed in Section III. Starting from a trial E1 distribution, cross sections were calculated in semi-classical approximation, convoluted with the detector response, and compared to the experimental data. In an iterative procedure, the E1 distribution was modified until the experimental data were reproduced. The resulting distribution is shown in Figure 4 in comparison to the

---

[†]Besides the strength distributions, the only free parameter in such a calculation is the range of the integration over the impact parameter. We use a sharp cut-off minimum impact parameter of b_{min}=9.6 fm relying on the ^{6}He interaction cross section measured in Ref. [33].

theoretical results of Refs. [31] and [7]. The differences between the two theoretical results may reflect the different interactions being used.

By integrating the experimental E1 strength distribution up to 5 MeV excitation energy, we derive that the energy-weighted Thomas-Reiche-Kuhn sum rule (S_{TRK}),

$$S_{TRK} = \frac{9}{4\pi} \frac{\hbar^2 e^2}{2m} \frac{NZ}{A},$$ (1)

is exhausted to $(10 \pm 2)\%$ (see table 2).

In a halo nucleus like ^{6}He, the most interesting comparison of the electromagnetic E1 strength function is provided by its relation to cluster sum rules. This is connected with the fact that the main mode of motion at low energies only contains the α particle and two neutrons.

The energy-weighted (EW) "cluster" sum rule [34,35] is obtained by splitting the strength of the dipole motion into that of the core, that of the halo nucleons, and that of the relative motion between core and halo. For a neutron halo, one obtains

$$S_{Clus}^{EW} = \frac{9}{4\pi} \frac{N_h Z_c^2 e^2}{AA_c} \frac{\hbar^2}{2m},$$ (2)

or the ratio

$$\frac{S_{Clus}^{EW}}{S_{TRK}} = \frac{Z_c N_h}{A_c N}$$ (3)

where indices c and h refer to core and halo, respectively. The E1 non-energy weighted (NEW) cluster sum rule [36,37] (see also [38]) reads

$$S_{Clus}^{NEW} = \frac{3}{4\pi} Z_c^2 e^2 <r_c^2> = \frac{3}{4\pi} Z_c^2 e^2 (\frac{N_h}{A_c})^2 <r_h^2>$$ (4)

where r_c (r_h) describes the distance between the center-of-mass of the core (halo neutrons) to that of the whole nucleus.

A comparison of the experimental E1 strength with the cluster sum rules may provide an interesting insight into the structure of ^{6}He ground-state wavefunction. From formula (4) one can see in a straightforward way that the non-energy-weighted sum rule is directly connected with the average distance between the α particle and the center of mass of the whole system. We can, in fact, here look into the geometry of the ground-state wave function from experimental data alone.

This statement is, of course, only valid if the energy-weighted strength distribution is close to what is given by the theoretical energy-weighted cluster sum rule. In Table II, we give the experimental values for the energy-weighted and non-energy-weighted strength for integration intervals up to 5.0 and 10.0 MeV, and compare the data with sum rule values and with the results of the three-body calculation of Ref. [7]. We observe good agreement between data and calculations for the excitation energy interval up to 5 MeV. For the 10 MeV

TABLE II. Experimental values (Exp.) for the integrated ($E^* \leq 5$ MeV and $E^* \leq 10$ MeV) non-energy-weighted ($\sum B(E1)$) and energy-weighted ($\sum E^* * B(E1)$) dipole strength. Corresponding theoretical values from Ref. and sum rule values are given for comparison.

Ref.		$\sum B(E1)$ $(e^2 \text{fm}^2)$	$\sum E^* * B(E1)$ $(e^2 \text{fm}^2 \text{MeV})$
Exp.	($E^* \leq 5$ MeV)	0.59 ± 0.12	1.9 ± 0.4
[7]	($E^* \leq 5$ MeV)	0.71	2.46
Exp.	($E^* \leq 10$ MeV)	1.2 ± 0.2	6.4 ± 1.3
[7]	($E^* \leq 10$ MeV)	1.02	4.97
Cluster Sum Rule		1.37 [7]	4.95
TRK Sum Rule			19.7

interval, moreover, both the experimental and the theoretical values almost exhaust the energy-weighted cluster sum rule. Thus, we may use the experimental B(E1) strength integrated over this energy interval from which, by means of equation (4), we deduce rms values $\sqrt{<r_c^2>}$ $= 1.12 \pm 0.13$ fm or $\sqrt{<r_h^2>} = 2.24 \pm 0.26$ fm. We may compare these results with theoretical three-body calculations summarized in Table 7 of Ref. [23] which gives the range of $\sqrt{<r_c^2>}$ between 1.18 to 1.29 fm. We may also compare the root-mean-square distance between the α particle and two valence neutrons, $r_{\alpha-2n} = 3.36 \pm 0.29$ fm. The theoretical results from different three-body models (see Table 3 in Ref. [39]) give the range for $r_{\alpha-2n}$ between 3.19 and 4.24 fm.

For further consolidation of the interpretation of a predominant electromagnetic excitation process in interactions of ^{6}He with the Pb target, the ^{6}He angular distribution was inspected. The polar scattering angle of ^{6}He was reconstructed from the measured momenta of the outgoing two neutrons and the α particle. The resulting angular distribution is shown in Figure 5 (left frame) in comparison with the semi-classical calculation using the experimentally derived E1-strength distribution adopting pure Coulomb trajectories. The impact parameter b used in the semi-classical formulation is related to the cm scattering angle ($\vartheta_{lab} \approx \vartheta_{cm}/1.04$ in the present case) for small angles

$$\vartheta_{cm} = \frac{2 Z_t Z_p e^2}{\beta^2 \gamma \mu} \frac{1}{b} \qquad (5)$$

where the indices t and p denote target and projectile quantities, and μ the reduced mass. Very good agreement is observed up to the grazing angle at around 19 mrad. From a comparison with the corresponding angular distribution from the C target, also shown in Figure 5, we infer that nuclear excitations take over at larger scattering angles.

B. Nuclear inelastic scattering

In the excitation energy spectrum of the Pb target, a small peak structure at $E^* = 1.8$ MeV, coinciding with the known $I^\pi = 2^+$ resonance, is observed. This peak becomes more pronounced in the correlation function also displayed in Figure 3. The width of this structure is also consistent with the known value [21], see Figure 1. The cross section amounts to (14 ± 4) mb, see Table I. The same structure, even more pronounced, is observed in the excitation energy spectrum obtained with the C target, again emphasized in the corresponding correlation function, see Figure 3. Its cross section is (4.0 ± 0.8) mb. The analysis of these cross sections obtained with the Pb and C target, performed in a manner outlined below, delivers deformation parameters being consistent with each other. The averaged value is $\delta_2 = (1.7 \pm 0.3)$ fm, which may be converted into B(E2, $0^+ \rightarrow 2^+$) = (3.2 ± 0.6) $e^2 \text{fm}^4$. This result, however, is model dependent, since it relies on a specific form of the transition densities and a specific relation between δ_2 and B(E2) values (for a discussion see below). We notice that a second 2^+ resonance located at $E^* = 4.3$ MeV and of 1.2 MeV width was predicted in Refs. [6,40] for which we find no clear experimental signature.

Apart from the 1.8 MeV resonance, both the excitation energy spectrum and the correlation function appear to be structureless. This smooth continuum cross section could be composed of various multipolarities. The C target is a selfconjugate isospin T=0 system and thus nuclear excitations of isovector modes in the T=1 nucleus ^{6}He, in particular dipole excitations, should be suppressed. On the other hand, however, as discussed in Ref. [41] and more recently in Ref. [42], isoscalar probes can induce isovector transitions, e.g. in nuclei with neutron excess, due to a different radial extent of proton and neutron matter distributions.

In order to explore the contributions to the experimentally observed nuclear cross section from various multipolarities, we performed an analysis using transition densities from various multipolarities thereby assuming that the observed transitions are of vibrational type. In principle, transition densities derived from microscopic models should be used. The following calculations, thus, should be considered as more schematic ones, aiming at a qualitative understanding rather than at a quantitative analysis.

In order to obtain nuclear cross sections, we performed coupled-channels calculations, the essentials of the method are described in Ref. [43]. Inelastic cross sections were calculated in a semiclassical approach adjusted to high energy scattering using the Coulomb potential and a nuclear optical potential. Effects of strong absorption were incorporated in the eikonal approximation. We rely on electric multipole strength distributions
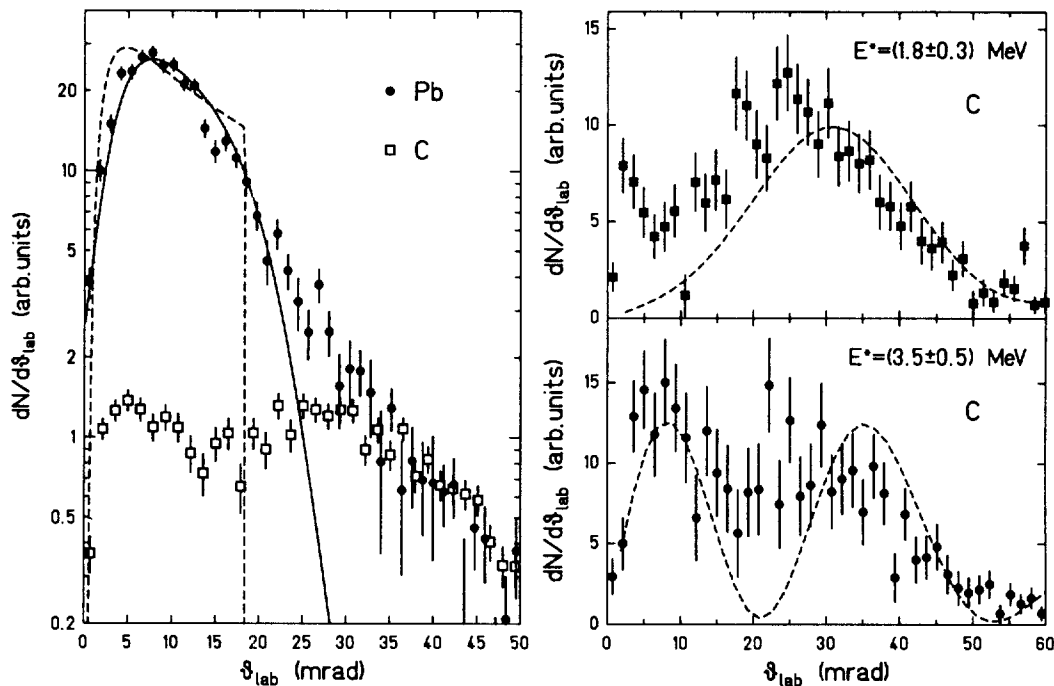
FIG. 5. Left: Angular distribution of ^{6}He obtained with the Pb and C target. The polar scattering angle ϑ_{lab} is constructed from the measured momenta of the outgoing two neutrons and the α particle. The dashed line reflects the angular distribution (Pb target) calculated in semi-classical approximation, using the experimentally determined E1 strength distribution, and adopting pure Coulomb trajectories. The solid line is obtained by convoluting the dashed line with the experimental resolution. Right: Angular distribution obtained with the C target and with different cuts on the excitation energy E^*. The upper part corresponds to the energy region of the 2^+ resonance at 1.80 MeV. The dashed curves represent calculated (see text) angular distributions for quadrupole (upper panel) and monopole (lower panel) transitions, normalized arbitrarily.

from three-body models, as described earlier. In order to describe nuclear excitations, the $B(E\lambda)$ values need to be converted into nuclear deformation parameters δ_λ. We used $\delta_1^2 = (\frac{3}{2\pi}\frac{ZN}{A})^{-2}B(E1)/e^2$ (dipole transitions) and $\delta_2^2 = (\frac{3}{4\pi}ZR)^{-2}B(E2)/e^2$ (quadrupole transitions) according to the Bohr-Mottelson particle-vibrator coupling model [44]. We are aware that these relations are model dependent and may be less appropriate in the case of halo nuclei with their differing mass and charge distributions.

Following the prescription given in Ref. [41], we use transition potentials $U_0(r)$, $U_1(r)$, and $U_2(r)$, for monopole, dipole, and quadrupole transitions, respectively.

$$U_0(r) = 3\ U(r) + r\ dU(r)/dr, \tag{6}$$

$$U_1(r) = \frac{3}{2}\ \frac{\Delta R}{R}\ (dU(r)/dr + \frac{R}{3}\ d^2U/dr^2), \tag{7}$$

$$U_2(r) = dU(r)/dr, \tag{8}$$

In these equations a power expansion in $\Delta R = R_n - R_p$ was used for the dipole mode which was also applied in Ref. [45] in analyzing neutron skins from isovector giant

dipole resonance excitations in inelastic α scattering. For the difference in proton and neutron radius, R_p and R_n respectively, we use an average value from that derived in Ref. [19] and in [20]. The optical potential $U(r)$ was derived from folding the ^{6}He and target nucleon densities applying the t-$\rho\rho$ approximation. For ^{6}He, we use a density distribution as derived in Ref. [19] on the basis of elastic proton scattering, and for the C and Pb targets modified Fermi distributions with parameters as quoted in Ref. [46]. The validity of the t-$\rho\rho$ approximation in applications with halo nuclei was discussed in Ref. [47].

By using the experimentally derived B(E1) strength distribution as shown in Figure 4, we obtain a cross section for the C target of about 4 mb, comprising only about 15% of the total experimental continuum cross section. Thus it seems evident, that transitions of other multipolarity contribute significantly. This may be considered as a first experimental evidence for low-lying multipole strength other than of dipole character in halo nuclei. So far, only low-lying dipole strength was known from experiments with ^{11}Li and ^{11}Be.

We estimated the contribution of quadrupole transitions on the basis of B(E2) strength distributions provided by three-body model calculations. For instance,

8

using the E2 strength distribution of Ref. [31], one obtains a cross section of 4 mb, i.e. again about 15 % of the measured cross section. As discussed above, the calculated cross section depends on the particular choice of the transition density, and one may question if the transition density given related to equation (8) is appropriate in case of halo-type matter distributions. Nevertheless, it appears that dipole and quadrupole transitions together cannot fully account for the measured total inelastic nuclear cross section. Thus, it seems conceivable that also other multipolarities contribute. In that respect, further information, at least of qualitative nature, can be obtained from the ^{6}He angular distribution. In the following, we compare experimental angular distributions with distributions calculated in DWBA using the eikonal approximation [47]. Figure 5 displays the angular distribution obtained with the C target by integrating the inelastic cross section (left frame, open symbols) and for two different excitation energy regions (right frames). In the right upper part the distribution is shown for an excitation energy where the $I^\pi = 2^+$ (1.80 MeV) resonance is located. A broad angular distribution is observed, centered around 25 mrad. We show the angular distribution calculated for an $I^\pi = 2^+$ transition in Figure 5 for comparison (dashed line), and we observe reasonable agreement. For the continuum part (3.0 MeV$\leq E^* \leq$ 4.0 MeV), a similar distribution, centered around 25–30 mrad is observed, but in addition, a considerable fraction of cross section appears close to zero degree. The angular distribution calculated for a monopole transition, also shown in the lower right part of Figure 5 (dashed line), exhibits a similar pattern. Thus, the observed continuum cross section may be attributed in part to monopole transitions for which low-lying strength is predicted as well from three-body models Refs. [7,31].

C. Two-body correlations

Finally, we present an analysis, aiming at an investigation of two-body correlations in the $\alpha + n + n$ channel. In Ref. [16], it was claimed that in high energy inelastic scattering, where a sudden approximation may become valid, initial state correlation among the two-body constituents in a Borromean system may prevail in the exit channel. In Figure 6, we present neutron-α and neutron–neutron relative energy spectra from the measurement with the Pb target. The data are compared with event simulations starting from the measured excitation energy and distributing the available kinetic energy between the α particle and the two neutrons according to standard phase space distributions. In both spectra, we find small deviations from the phase space distributions. In the neutron-α spectrum, a slight excess is observed coinciding in energy with the ^{5}He ground state resonance. In the neutron–neutron spectrum very low relative ener-

gies appear to be enhanced, qualitatively in accord with the known, very low-lying virtual state in the neutron–neutron channel. The deviations from phase space distributions may thus be caused by final state interactions. To find out to which extent initial state correlations are reflected as well, would require substantial theoretical efforts in analyzing the data, going beyond the scope of this paper. We note that also relative angle spectra between two-body constituents were inspected and again, only minor modifications of the respective phase space distributions were found. In particular the neutron–neutron relative-angle distribution shows a slight enhancement around a zero relative angle, in line with the enhancement at low relative energies. Also, corresponding correlations obtained with the C target exhibit qualitatively very similar features.

D. Astrophysical aspects

We finally like to point out the astrophysical aspects inherent in our experimental data. In the past years it was discussed that the postcollapse phase in a type II supernova may offer the "ideal site" for the r-process forming the heaviest elements. In the preceding α process, elements up to masses A $\leq$ 100 are built. The bottleneck in this nucleosynthesis process is the formation of nuclei with A $\geq$ 9 from nucleons and α particles. Two-step processes, such as ^{4}He$(2n, \gamma)^6$He and ^{6}He$(2n, \gamma)^8$He were considered to be potentially relevant in bridging the instability gaps at A = 5 and A = 8, see Refs. [17,18]. It is presently believed that the two-neutron capture cannot compete with the $(\alpha n, \gamma)$ process in a type II supernova scenario, but other scenarios such as production of r-process elements in the coalescence of two neutron stars are still under discussion for which the relevance of two-neutron capture processes is yet to be explored [48]. In any case, it is certainly of interest to check experimentally the model-dependent assumptions on which such conclusions are based so far. As far as the ^{4}He$(2n, \gamma)^6$He reaction is concerned, one of the contributing mechanisms is the formation of the ^{5}He ground state resonance as an intermediate state, followed by radiative capture of a second neutron with creation of the ^{6}He ground state. Non-resonant mechanisms involving E1 photoabsorption, however, were considered as well. We note that our data obtained with the Pb target, discussed in Section IV.A, comprise exactly the inverse process, i.e. absorption of a (virtual) γ quantum followed by two-neutron emission.

First, we were able to extract a B(E2, $0^+ \rightarrow 2^+$) = (3.2 ± 0.6) e^2fm^4 value, although in a model dependent way. It can be compared, for instance, with the one used in the model calculation of Goerres et al. [18]. There, a value of 2.85 e^2fm^4 was adopted, which our data now basically confirm.
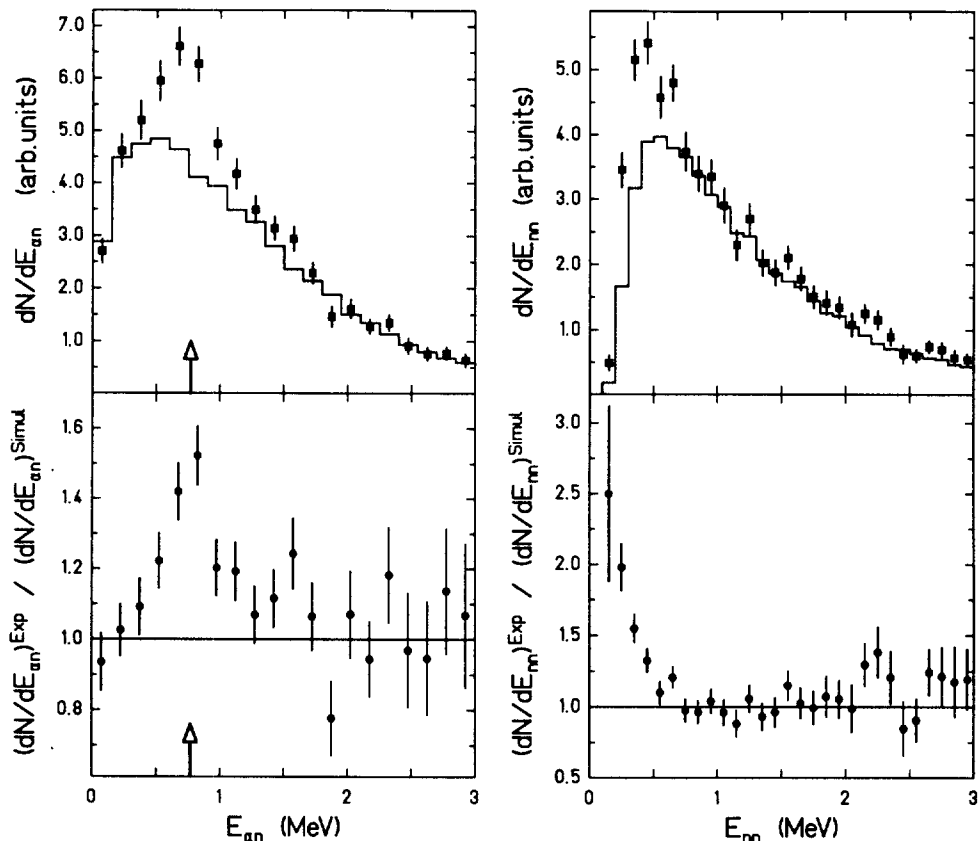
FIG. 6. Top: Spectra of relative energy between α particle and neutron (left) and between two neutrons (right), observed after break-up of ^{6}He in the Pb target. The solid curves represent the calculated phase space distributions. Bottom: Ratio between the observed relative energy distributions and calculated phase space distributions. The energy of the ^{5}He ground state resonance is indicated by an arrow.

But, moreover, non-resonant transitions can now be estimated on the basis of our data. In fact, Efros et al. [17] consider the process of a non-resonant electric dipole transition as the main contribution to the second step of the reaction, i.e. the neutron capture leading from ^{5}He to ^{6}He. By relying on B(E1) strength distributions from a three-body model, they obtain an enhancement of three orders of magnitude of the non-resonant mechanism in comparison with the resonant one via the ^{6}He $I^\pi = 2^+$ (1.80 MeV) resonance. It is straightforward to transform our experimental dB(E1)/dE* distribution into a photoabsorption cross section which can be compared with the one used in the calculation of Efros et al., see Figure 3 of Ref. [17]. Their photoabsorption cross section for the ^{6}He$(\gamma, n)^5$He reaction peaks at around 2.3 MeV with a value of 0.12 mb; the photoabsorption cross section integrated up to 8 MeV excitation energy amounts to about 0.4 mb·MeV. From our data, we deduce a total photoabsorption cross section integrated up to 8 MeV of (16 ± 3) mb·MeV. In comparison with the calculation of Ref. [17], however, only that fraction of the cross section is relevant which proceeds via the ^{5}He ground state reso-

nance. We may obtain an estimate of that by inspecting the relative energy spectrum of the $\alpha - n$ subsystem, shown in Figure 6. From this spectrum, we deduce that about 10 % lead to the ^{5}He resonance. Assuming that the ^{5}He formation is independent of the γ energy, we can derive a rough estimate of the photoabsorption cross section for the ^{6}He$(\gamma, n)^5$He reaction amounting to about 1.6 mb·MeV. This value is of the same order of magnitude as the one used by Efros et al., given above.

Currently, we attempt a more detailed analysis of the neutron capture process from our data together with corresponding results which we obtained with a ^{8}He beam, thus spanning the whole sequence ^{4}He $\rightarrow$ ^{6}He $\rightarrow$ ^{8}He.

V. CONCLUSION

By using an energetic secondary beam of ^{6}He produced in a fragmentation reaction, we have investigated the inelastic break-up into two neutrons and the ^{4}He core. We were able to derive quantitative results for the E1 continuum strength distribution and for the E2 transition

10

probability to the $I^\pi=2^+$ resonance in ^{6}He. Both results are not only of interest with regard to the neutron halo structure of ^{6}He, but are relevant as well in the stellar nucleosynthesis process. In the latter context, we could show that even information on photoabsortion cross sections in reactions such as ^{6}He$(\gamma, n)^5$He, involving a β- and a particle-unstable nucleus, can be deduced, utilizing two-body correlations observed in the break-up channel. A large fraction of the dipole strength, exhausting that given by cluster sum rules, is localized at low excitation energies (≤ 10 MeV). This observation allowed to deduce information on the geometry of the ^{6}He ground state wave function, i.e. to determine the root-mean-square distance between core and halo neutrons. In addition, we obtain first experimental evidence for low-lying strength of multipolarity other than dipole, most likely of monopole and quadrupole type. The data were compared with recent, most advanced three-body model calculations, elucidating the specific structure of Borromean-type nuclei.

[1] G. F. Bertsch and J. Foxwell, Phys. Rev. **C41**, 1330 (1990).

[2] S. A. Fayans, Phys. Lett. **B267**, 443 (1991).

[3] B. V. Danilin, M. V. Zhukov, J. S. Vaagen and J. M. Bang, Phys. Lett. **B302**, 129 (1993).

[4] M. Yokoyama, T. Otsuka and N. Fukunishi, Phys. Rev. **C52**, 1122 (1995).

[5] I. Hamamoto and H. Sagawa Phys. Rev. **C53**, R1492 (1996).

[6] B. V. Danilin, J. S. Vaagen, S. N. Ershov, H. Heiberg-Andersen, I. J. Thompson and M. V. Zhukov, Phys. Rev.

55, R577 (1997).

[7] B. V. Danilin, I. J. Thompson, J. S. Vaagen, M. V. Zhukov, Nucl. Phys. **A632**, 383 (1998).

[8] D. Sackett, K. Ieki, A. Galonsky, C. A. Bertulani, H. Esbensen, J. J. Kruse, W. G. Lynch, D. J. Morrissey, B. M. Sherrill, H. Schulz, A. Sustich, J. A. Winger, F. Deák, Á. Horváth, Á. Kiss, Z. Seres, J. J. Kolata, R. E. Warner and D. Humphrey, Phys. Rev. **C48**, 118 (1993).

[9] S. Shimoura, T. Nakamura, M. Ishihara, N. Inabe, T. Kobayashi, T. Kubo, R.H. Siemssen, I. Tanihata and Y. Watanabe, Phys. Lett **B348**, 29 (1995).

[10] M. Zinser, F. Humbert, T. Nilsson, W. Schwab, H. Simon, T. Aumann, M. J. G. Borge, L. V. Chulkov, J. Cub, Th. W. Elze, H. Emling, H. Geissel, D. Guillemaud-Mueller, P. Hansen, R. Holzmann, H. Irnich, B. Jonson, J. V. Kratz, R. Kulessa, Y. Leifels, A. Magel, A. C. Mueller, G.Münzenberg, F. Nickel, G. Nyman, A. Richter, K. Riisager, C. Scheidenberger, G. Schrieder, K. Stelzer, J.Stroth, A. Surowiec, O. Tengblad, E. Wajda and E. Zude, Nucl. Phys. **A619**, 151 (1997).

[11] T. Nakamura, S. Shimoura, T. Kobayashi, T. Teranishi, K. Abe, N. Aoi, Y. Doki, M. Fujimaki, N. Inabe, N. Iwasa, K. Katori, T. Kubo, H. Okuno, T. Suzuki, I. Tanihata, Y. Watanabe, A. Yoshida and M. Ishihara, Phys. Lett. **B331**, 296 (1994).

[12] C. H. Dasso, S. M. Lenzi and A. Vitturi, Nucl. Phys. **A611**, 124 (1996).

[13] P. G. Hansen and B. Jonson, Europhys. Lett. **4**, 409 (1987).

[14] K. Ikeda, INS Report JHP-7 (1988).

[15] J. Chambers, E. Zaremba, J. P. Adams and B. Castel, Phys. Rev. **C50**, R2671 (1994).

[16] M. V. Zhukov, L. V. Chulkov, B.V. Danilin and A. A. Korsheninnikov, Nucl. Phys. **A533**, 428 (1991).

[17] V. Efros, W. Balogh, H. Herndl, R. Hofinger and H. Oberhummer, Z. Phys. **A355**, 101 (1996).

[18] J. Görres, H. Herndl, I. J. Thompson and M. Wiescher, Phys. Rev. **C52**, 2231 (1995).

[19] G. Alkhazov, M. Andronenko, A. Dobrovolsky, P. Egelhof, G. Gavrilov, H. Geissel, H. Irnich, A. Khanzadeev, G. Korolev, A. Lobodenko, G. Münzenberg, M. Mutterer, S. Neumaier, F. Nickel, W. Schwab, D. Seliverstov, T. Suzuki, J. Theobald, N. Timofeev and A. V. V. Yatsoura, Phys. Rev. Lett. **78**, 2313 (1997).

[20] I. Tanihata, H. Hirata, T. Kobayashi, S. Shimoura, K. Sugimoto and H. Kubo, Phys. Lett **B289**, 261 (1992).

[21] F. Ajzenberg-Selove, Nucl. Phys. **A490**, 1 (1988).

[22] A. Csótó, Phys. Rev. **C48**, 165 (1993).

[23] M. V. Zhukov, B. V. Danilin, D. Fedorov, J. Bang, I. J. Thompson and J. S. Vaagen, Phys. Rep. **231**, 151 (1993).

[24] B. Pudliner, V. R. Pandharipande, J. Carlson, S. C. Pieper and R. B. Wiringa, Phys. Rev. **C56**, 1720 (1997).

[25] J. Wurzer and H. Hofmann, Phys. Rev. **C55**, 688 (1997).

[26] H. Geissel, P. Armbruster, K. Behr, A. Brünle, K. Brukard, M. Chen, H. Folger, B. Franczak, H. Keller, O. Klepper, B. Langenbeck, F. Nickel, E. Pfeng, M. Pfützner, E. Roeckl, K. Rykaczewski, I. Schall, D. Schardt, C. Sheidenberger, K.-H. Schmidt, A. Schröter, T. Schwab, K. Sümmerer, M. Weber,

G. Münzenberg, T. Brohm, H.-G. Clerc, M. Fauerbach, J.-J. Gaimard, A. Grewe, E. Hanelt, B. Knödler, M. Steiner, B. Voss, J. Weckenmann, C. Ziegler, A. Magel, H. Wollnik, J. Dufour, Y. Fujita, D. Viera and B. M. Sherrill, Nucl. Instr. and Meth. **B70**, 286 (1992).

[27] T. Blaich, T. W. Elze, H. Emling, H. Freiesleben, K. Grimm, W. Henning, R. Holzmann, G. Ickert, J. G. Keller, H. Klingler, W. Kneissl, R. König, R. Kulessa, J. V. Kratz, D. Lambrecht, J. S. Lange, Y. Leifels, E. Lubkiewicz, M. Proft, W. Prokopowicz, C. Schütter, R. Schmidt, H. Spies, K. Stelzer, J. Stroth, W. Walús, E. Wajda, H. J. Wollersheim, M. Zinser and E. Zude, Nucl. Instr. and Meth. **A314**, 136 (1992).

[28] L. V. Chulkov, T. Aumann, D. Aleksandrov, L. Axelsson, T. Baumann, M. J. G. Borge, R. Collatz, J. Cub, W. Dostal, B. Eberlein, Th. W. Elze, H. Emling, H. Geissel, V. Z. Goldberg, M. Golovkov, A. Grünschloß, M. Hellström, J. Holeczek, R. Holzmann, B. Jonson, A. A. Korsheninnikov, J. V. Kratz, G. Kraus, R. Kulessa, Y. Leifels, A. Leistenschneider, T. Leth, I. Mukha, G. Münzenberg, F. Nickel, T. Nilsson, G. Nyman, B. Petersen, M. Pfützner, A. Richter, K. Riisager, C. Scheidenberger, G. Schrieder, W. Schwab, H. Simon, M. H. Smedberg, M. Steiner, J. Stroth, A. Surowiec, T. Suzuki and O. Tengblad, Phys. Rev. Lett. **79**, 201 (1997).

[29] D. Aleksandrov, T. Aumann, L. Axelsson, T. Baumann, M. Borge, L. V. Chulkov, J. Cub, W. Dostal, B. Eberlein, Th. W. Elze, H. Emling, H. Geissel, V. Z. Goldberg, M. Golovkov, A. Grünschloß, M. Hellström, J. Holeczek, R. Holzmann, B. Jonson, A. A. Korsheninnikov, J. V. Kratz, G. Kraus, R. Kulessa, Y. Leifels, A. Leistenschneider, T. Leth, I. Mukha, G. Münzenberg, F. Nickel, T. Nilsson, G. Nyman, B. Petersen, M. Pfützner, A. Richter, K. Riisager, C.Scheidenberger, G. Schrieder, W. Schwab, H. Simon, M. H. Smedberg, M. Steiner, J. Stroth, A. Surowiec, T. Suzuki, O. Tengblad and M. V. Zhukov, Nucl. Phys. **A633**, 234 (1998).

[30] G. F. Bertsch, K. Hencken and H. Esbensen, Phys. Rev. **C57**, 1366 (1998).

[31] A. Cobis, D. Fedorov and A. Jensen, Phys. Rev. Lett. **79**, 2411 (1997).

[32] A. Winther and K. Alder, Nucl. Phys. **A319**, 518 (1979).

[33] I. Tanihata, H. Hamagaki, O. Hashimoto, S. Nagamiya, Y. Shida, N. Yoshikawa, O. Yamakawa, K. Sugimoto, T. Kobayashi, D. Greiner, N. Takahashi and Y. Nojiri, Phys. Lett. **B160**, 380 (1985).

[34] Y. Alhassid, M. Gai and G. F. Bertsch, Phys. Rev. Lett. **49**, 1482 (1982).

[35] H. Sagawa and M. Honma, Phys. Lett. **B251**, 17 (1990).

[36] B.V. Danilin, M. V. Zhukov, J. S. Vaagen, J.M. Bang, Phys. Lett. **B302**, 129 (1993).

[37] H. Esbensen, G. F. Bertsch, Nucl. Phys, **A542**, 310 (1992).

[38] J. M. Bang, L. S. Ferreira, E. Maglione, Europhys. Lett. **18**, 679 (1992).

[39] S. Funuda, H. Kameyama, Y. Sakuragi, Nucl. Phys. **A575**, 93 (1994).

[40] S. Ershov, T. Rodge, B. V. Danilin, J. S. Vaagen, I. J. Thompson and F. Gareev, Phys. Rev. **C56**, 1483 (1997).

[41] G. Satchler, Nucl. Phys. **A472**, 215 (1987).

[42] C. Dasso, H. Sofia, S. Lenzi, M. Nagarajan and A. Vitturi, Nucl. Phys. **A627**, 349 (1997).

[43] C. A. Bertulani, L. F. Canto, M. S. Hussein and A. F. R. de Toledo Piza, Phys. Rev. **C53**, 334 (1996).

[44] A. Bohr and B. R. Mottelson, Nuclear Structure, vol. 2 (Benjamin, Reading, 1975).

[45] A. Krasznahorkay, J. Bacelar, A. Bordewijk, S. Brandenburg, A. Buda, G. van't Hof, M. Hofstee, S. Kato, T. Poelhekken, S. van der Werf, A. van der Woude, M. Harakeh and N. Kalantar-Nayestanaki, Phys. Rev. Lett. **66**, 1287 (1991).

[46] H. De Vries, C. W. De Jager and C. De Vries, At. Data Nucl. Data Tables **36**, 495 (1987).

[47] C. A. Bertulani and H. Sagawa, Nucl. Phys. **A588**, 667 (1990).

[48] H. Oberhummer, private communication